Biochemical and Biophysical Research Communications 450 (2014) 1452–1457

Contents lists available at ScienceDirect

Biochemical and Biophysical Research Communications

journal homepage: www.elsevier.com/locate/ybbrc

Activation-induced structural change in the GluN1/GluN3A excitatory glycine receptor

Dilshan Balasuriya, Hirohide Takahashi, Shyam Srivats, J. Michael Edwardson *

Department of Pharmacology, University of Cambridge, Tennis Court Road, Cambridge CB2 1PD, United Kingdom

ARTICLE INFO

Article history:
Received 27 June 2014
Available online 10 July 2014

Keywords:
Ionotropic glutamate receptor
NMDA receptor
Excitatory glycine receptor
Receptor activation
Atomic force microscopy

ABSTRACT

Unlike GluN2-containing *N*-methyl-D-aspartate (NMDA) receptors, which require both glycine and glutamate for activation, receptors composed of GluN1 and GluN3 subunits are activated by glycine alone. Here, we used atomic force microscopy (AFM) imaging to examine the response to activation of the GluN1/GluN3A excitatory glycine receptor. GluN1 and GluN3A subunits were shown to interact intimately within transfected tsA 201 cells. Isolated GluN1/GluN3A receptors integrated into lipid bilayers responded to addition of either glycine or D-serine, but not glutamate, with a ~1 nm reduction in height of the extracellular domain. The height reduction in response to glycine was abolished by the glycine antagonist 5,7-dichlorokynurenic acid. Our results represent the first demonstration of the effect of activation on the conformation of this receptor.

1. Introduction

N-methyl-D-aspartate (NMDA) receptors operate as obligate heterotetramers that usually contain two GluN1 subunits and either two GluN2 subunits or one GluN2 and one GluN3 subunit [1]. While GluN1 and GluN3 bind glycine and D-serine, GluN2 binds glutamate; hence, activation of GluN2-containing receptors requires both glycine/D-serine and glutamate. In contrast, receptors composed of GluN1 and GluN3 subunits can be activated by glycine in the absence of glutamate [2,3]. These GluN1/GluN3 excitatory glycine receptors also lack the high Ca^{2+} permeability and strong voltage-dependent Mg^{2+} block shown by conventional GluN2-containing NMDA receptors [2,4].

We have recently used atomic force microscopy (AFM) imaging of GluN1/GluN2A NMDA receptors integrated into lipid bilayers to reveal a rapid activation-induced conformational change in the extracellular domain of the receptor [5]. In the present study, we have isolated receptors composed of GluN1 and GluN3A subunits. We show that the GluN1/GluN3 receptor undergoes a conformational change in response to either glycine or D-serine alone, but does not respond to glutamate.

2. Materials and methods

2.1. Cell culture

tsA 201 and HEK-293 cells were grown in Dulbecco's modified Eagle's medium supplemented with 10% (v/v) fetal bovine serum, 100 μg/ml of streptomycin and 100 units/ml of penicillin in an atmosphere of 5% CO_2/air.

2.2. Constructs

The following constructs were used: wild type (WT) rat GluN1 in the vector pcDNA3.1; GluN1 with a hemagglutinin (HA)/His_8 tag between residues 416 and 417 in the agonist binding domain (ABD), also in pcDNA3.1; wild type rat GluN3A in the vector pcINeo; and GluN3A with an N-terminal Myc epitope tag, also in pcINeo.

2.3. In situ proximity ligation assay

tsA 201 cells growing on lysine- and collagen-coated glass coverslips were co-transfected with 1.5 μg each of DNA encoding GluN1-HA and WT GluN3A. Cells were incubated for 24 h at 37 °C to allow protein expression, and the proximity ligation reaction was carried out according to the manufacturer's instructions (Olink Bioscience). Antibodies used were rabbit polyclonal anti-HA (Sigma, H6908) plus either mouse monoclonal anti-GluN3A (Thermo Scientific, K35/40.1, raised against residues 780–914) or,

Abbreviations: ABD, agonist binding domain; AFM, atomic force microscopy; DCKA, 5,7-dichlorokynurenic acid; HA, hemagglutinin; HBS, HEPES-buffered saline; HEK, human embryonic kidney; NMDA, *N*-methyl-D-aspartate; PC, L-α-phosphatidylcholine; PS, L-α-phosphatidylserine; SDS–PAGE, SDS–polyacrylamide gel electrophoresis; WT, wild type.

* Corresponding author. Fax: +44 1223 334100.
E-mail address: jme1000@cam.ac.uk (J.M. Edwardson).

http://dx.doi.org/10.1016/j.bbrc.2014.07.009
0006-291X/

as a negative control, mouse monoclonal anti-V5 (Life Technologies, R960-25). Cells were imaged by confocal laser scanning microscopy.

2.4. Assay for receptor function

HEK-293 cells growing on poly-L-lysine-coated coverslips were transfected with DNA encoding WT GluN1 (0.5 μg) and either WT or Myc-tagged GluN3A (1.5 μg), using polyethylenimine as the transfection reagent. This 1:3 DNA ratio was used to minimize the likelihood that GluN1 homotetramers would be generated. DNA encoding Red Fluorescent Protein (RFP; 0.5 μg) was also included as a marker for transfection. After 48 h, cells were incubated in buffer (140 mM NaCl, 5 mM KCl, 1 mM $MgCl_2$, 2 mM $CaCl_2$, 10 mM glucose and 10 mM HEPES, pH 7.3) containing 2 μM Fluo-4 AM at room temperature for 1 h. The solution was then replaced with dye-free buffer to enhance the de-esterification of the Fluo-4 AM. The cells were imaged by confocal microscopy using a 40× oil immersion objective with a 488 nm laser to excite the Fluo-4 and a 543 nm laser to detect RFP. The imaging frequency was 1 Hz. Cells were treated with glycine (200 μM) in the absence and presence of the glycine site antagonist 5,7-dichlorokynurenic acid (DCKA; 1 mM). Changes in Fluo-4 fluorescence were detected using the ImageJ 'time series analyzer' V2.0 plug-in. Fmax was measured by saturating the dye with 10 mM Ca^{2+} in buffer containing 0.1% (v/v) Triton X-100. Transfection efficiency was typically ~50%, and ~25 RPF-positive cells were included in each field of view.

2.5. Receptor isolation

tsA 201 cells were transfected with DNA using calcium phosphate precipitation. In all cases, 250 μg of DNA was used to transfect 5 × 162 cm^2 flasks. For co-transfections of GluN1 and Myc-GluN3A, 125 μg of DNA for each construct were used. After transfection, cells were incubated for 48 h at 37 °C to allow protein expression. Transfected cells were grown to confluence and solubilized in 1% (v/v) Triton X-100 for 1 h at 4 °C before centrifugation at 62,000*g* in order to remove all insoluble material. Solubilized extracts were incubated with anti-Myc-agarose beads (Sigma) for 3 h. The beads were then washed extensively before the bound protein was eluted with Myc peptide (100 μg/ml). The eluted samples were analyzed by SDS–polyacrylamide gel electrophoresis (SDS–PAGE), followed by silver staining and/or immunoblotting using mouse monoclonal anti-GluN1 (Abcam, ab134308, S308-48, raised against amino acids 42–361) or mouse monoclonal anti-GluN3A (as above) primary antibody followed by horseradish peroxidase-conjugated goat anti-mouse secondary antibody (BioRad). Immunopositive bands were visualized using enhanced chemiluminescence.

2.6. Integration of receptors into liposomes

Chloroform solutions of L-α-phosphatidylcholine (PC) and brain L-α-phosphatidylserine (PS; Avanti Polar Lipids) were mixed at a molar ratio of 3:1. The chloroform was then evaporated under a stream of nitrogen gas, and the lipids were mixed with 200 μl of purified receptor in 2% 3-[(3-cholamidopropyl) dimethylammonio]propanesulfonate (Sigma). The mixture was dialysed at 4 °C against HEPES-buffered saline (HBS; 100 mM NaCl; 20 mM HEPES–NaOH, pH 7.6) for 3 days, with several buffer changes. The resulting liposome suspension was deposited onto freshly-cleaved mica disks. After a 3-min adsorption, the sample was rinsed with HBS containing 1 mM $CaCl_2$ to remove unadsorbed liposomes, and then transferred to the atomic force microscope.

2.7. AFM imaging

AFM imaging under fluid was carried out at room temperature (20 °C) using a Bruker Multimode atomic force microscope. All images were collected in 'tapping' mode, using the B triangle of a SNL-10 silicon nitride probe (Bruker). The cantilevers (with a typical spring constant of 0.12 N/m) were tuned to 10–20% below the peak of the resonance frequency, generally found between 15 and 30 kHz. The drive amplitude was set to generate a root-mean-square amplitude of 0.5 V. The microscope was engaged with a 0-nm scan area to allow for tuning. The setpoint was adjusted to the highest setting that allowed imaging with little noise, to minimize the force applied to the sample. Images were captured at a scan rate of 2 Hz, and with 512 scan lines per area. Data analysis was performed using the Nanoscope III software.

2.8. Statistical analysis

Histograms were drawn with bin widths chosen according to Scott's equation:

$$\text{Bin width} = 3.5\,\sigma/n^{1/3} \quad (1)$$

where σ is an estimate of the standard deviation and n is the sample size [6]. Where Gaussian curves were fitted to the data, the number of curves was chosen to maximize the r^2 value while giving significantly different means using Welch's *t*-test for unequal sample sizes and unequal variances [7]. The significance of differences between Gaussian distributions was determined using a two-sample *t*-test. $P < 0.05$ was taken as significant. All errors are S.E.M.

3. Results

An *in situ* proximity ligation assay was carried out to determine whether GluN1 and GluN3A interact in intact tsA 201 cells. Cells were co-transfected with DNA encoding GluN1-HA/His_8 and WT GluN3A. The assay uses two secondary antibodies, each bearing a short DNA strand [8]. When the secondary antibodies are brought into close proximity (<40 nm) by binding to their relevant primary antibodies (in this case rabbit anti-HA and a mouse anti-GluN3A that recognizes the extracellular loop between transmembrane regions 3 and 4), the DNA strands hybridize with an additional circle-forming oligodeoxynucleotide. Ligation then creates a complete circularized oligodeoxynucleotide, and rolling circle amplification increases the amount of circular DNA several 100-fold. The DNA is then visualized using a fluorescent probe. The assay gave a bright signal with cells co-expressing GluN1-HA/His_8 and GluN3A (Fig. 1A); however, there was no signal when the anti-GluN3A antibody was replaced by a mouse anti-V5 antibody (Fig. 1B), even though the cell monolayer was almost confluent, as can be seen in the corresponding brightfield image (Fig. 1C). Hence, GluN1 interacts with GluN3A within intact cells.

Given that we planned to isolate the GluN1/GluN3A receptor by immunoaffinity chromatography using a Myc epitope tag on GluN3A, we first checked that the tag does not affect the functional properties of the receptor. To do this we co-transfected HEK-293 cells with DNA encoding WT GluN1 and either WT or Myc-tagged GluN3A, and measured the Ca^{2+} responses of the cells to addition of glycine, using the fluorescent Ca^{2+} indicator, Fluo-4. As shown in Fig. 2A, addition of glycine (200 μM) to the co-transfected cells elicited a small but clear Ca^{2+} signal, as previously shown with GluN1/GluN3 receptors endogenously expressed in CNS myelin [9]. Importantly, the presence of the N-terminal Myc tag on GluN3A did not affect the Ca^{2+} response to glycine. As expected, cells expressing GluN1/WT GluN3A or GluN1/Myc-GluN3A did not respond to glycine in the presence of the glycine site antagonist

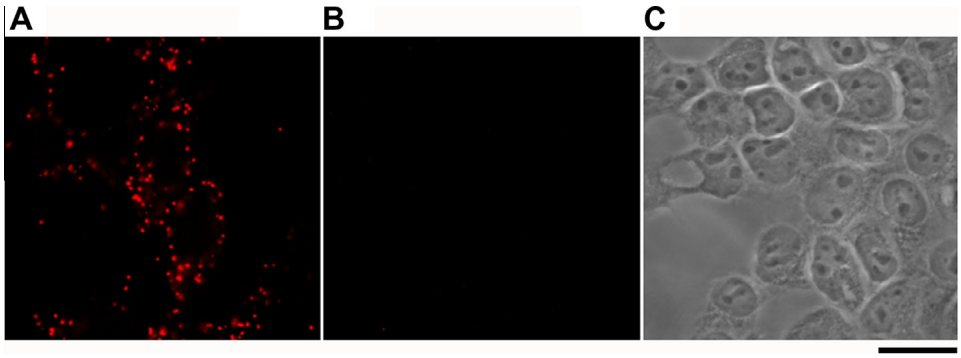

Fig. 1. *In situ* proximity ligation demonstrates an intracellular interaction between GluN1 and GluN3A. (A) tsA 201 cells were co-transfected with DNA encoding GluN1-HA (ABD) and WT GluN3A. Cells were fixed, permeabilized and incubated with primary antibodies (mouse monoclonal anti-GluN3A and rabbit polyclonal anti-HA) followed by anti-mouse (+) and anti-rabbit (−) proximity ligation secondary antibodies. The proximity ligation assay was then carried out. Scale bar, 20 μm. (B) As in (A), except that mouse monoclonal anti-GluN3A was replaced by mouse monoclonal anti-V5. (C) Brightfield image of the same area as that shown in (B).

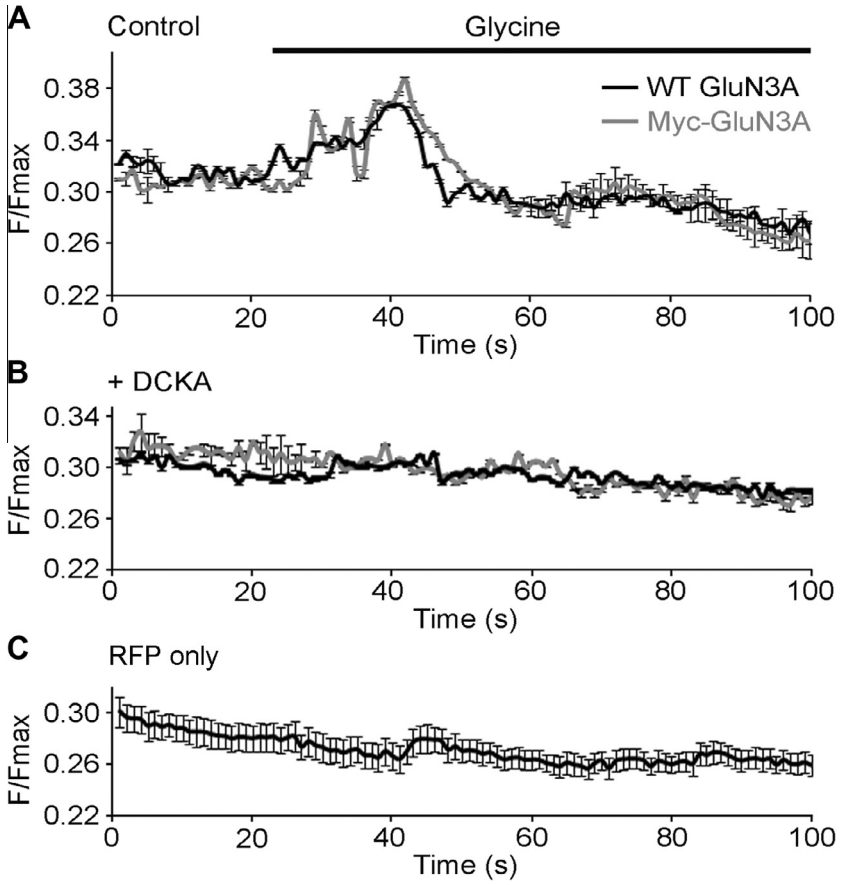

Fig. 2. Functional activity of the GluN1/GluN3A receptor. HEK-293 cells were co-transfected with WT GluN1 and either WT (black lines) or Myc-tagged (gray lines) GluN3A, together with RFP as a marker for transfection. Ca^{2+} responses of the cells to addition of glycine (200 μM, present during the time indicated by the bar) were measured using the fluorescent Ca^{2+} indicator, Fluo-4 in the absence (A) or presence (B) of the antagonist DCKA (1 mM). The Ca^{2+} response of cells expressing RFP only was also assessed (C). Error bars represent S.E.M. for areas on three coverslips ($n = 3$), each containing ~25 RFP-positive cells.

DCKA (1 mM; Fig. 2B), and glycine did not elicit a Ca^{2+} signal in cells expressing RFP only (Fig. 2C). On the basis of these results, we conclude that Myc-tagged GluN3A is fully functional.

tsA 201 cells were co-transfected with DNA encoding WT GluN1 and Myc-GluN3A, and protein was isolated from the transfected cells by anti-Myc affinity chromatography. Analysis of an isolated protein sample on a silver stained gel revealed two bands of almost equal intensity at ~120 and ~140 kDa (Fig. 3A, arrows). Immunoblotting using appropriate anti-subunit antibodies indicated that these two bands were GluN1 and GluN3A, respectively. Hence, GluN1 was robustly co-isolated with GluN3A. Contaminant bands were also seen on the silver stained gel. Isolated receptors were integrated into liposomes (PC:PS, 3:1). The proteoliposomes were deposited onto a mica disk to produce a supported proteolipid bilayer. AFM imaging of this bilayer under fluid revealed a smooth layer containing protein particles (Fig. 3B). Sections through the breaks in the bilayer indicated a height above the mica support of approximately 4 nm, as seen previously [5]. Imaging of a num-

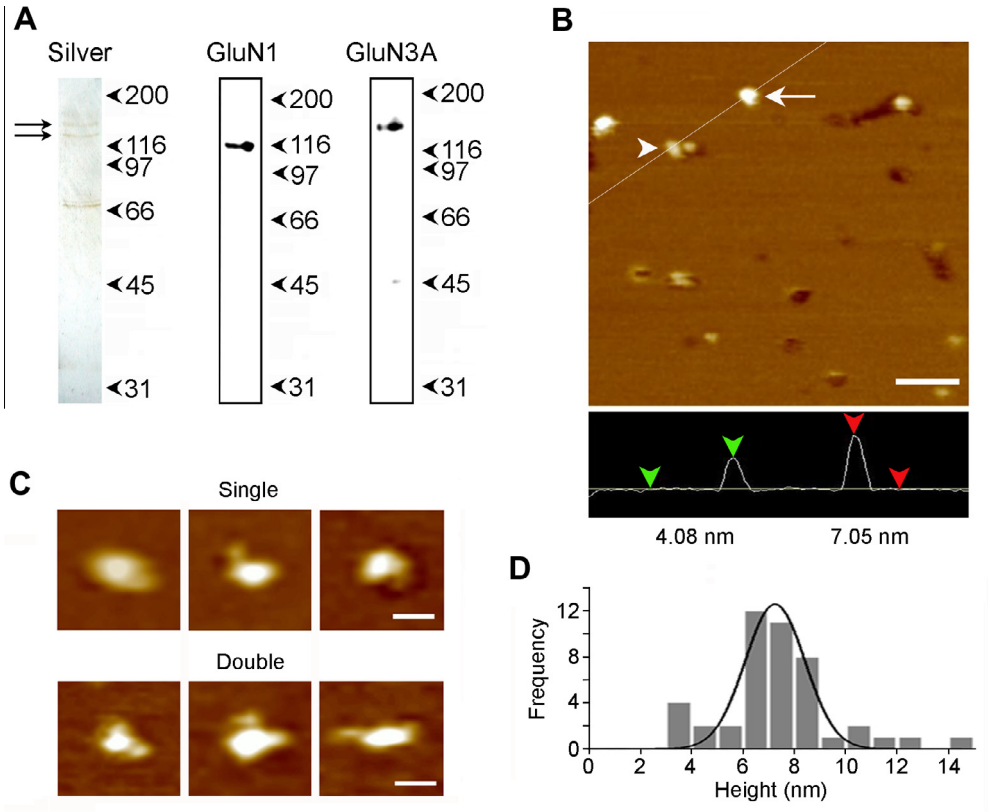

Fig. 3. Isolation and bilayer integration of GluN1/GluN3A receptors. (A) Proteins isolated from cells co-expressing WT GluN1 and GluN3A-Myc by anti-Myc immunoaffinity chromatography were analyzed by SDS–PAGE followed by either silver staining or immunoblotting using mouse monoclonal anti-GluN1 or anti-GluN3A antibodies. The silver stained gel of the isolated protein (left panel) shows bands at ~120 and ~140 kDa (arrows). Immunoblotting using anti-subunit antibodies demonstrated that these bands were GluN1 and GluN3A, respectively (center and right panels). (B) AFM image of a bilayer containing untreated receptors. Scale bar, 100 nm; height range 0–20 nm. A section through the bilayer, taken at the position indicated by the line, is shown below. (C) Zoomed images of receptors decorated either singly (upper panels) or doubly (lower panels) by anti-GluN1 antibodies. Scale bar, 50 nm; height range 0–20 nm. (D) Frequency distribution of heights of antibody-decorated receptor particles. A fitted Gaussian curve is overlaid on the histogram.

ber of the bilayer-integrated particles revealed two distinct height populations at around 4 nm and around 7 nm; for example, Fig. 2B shows two particles of heights 4.1 nm (arrowhead) and 7.0 nm (arrow).

To further characterize the two particle populations, the proteoliposomes were incubated with an antibody against the ABD of the GluN1 subunit (described above). Fig. 3C shows a gallery of particles that were either singly (top panels) or doubly (bottom panels) decorated by antibodies. The frequency distribution of heights of the antibody-decorated particles (determined as illustrated in Fig. 2B) had a peak at 7.2 ± 0.3 nm (n = 45; Fig. 3D), demonstrating that the taller particles represent the extracellular region of the receptor. The smaller particles likely represent a mixture of incompletely assembled receptors, receptors integrated intracellular face up, and impurities.

Fig. 4A shows a frequency distribution of the heights of particles in an untreated proteolipid bilayer. As mentioned above, the distribution had two peaks, at 4.0 ± 0.2 nm (n = 51) and 6.8 ± 0.2 nm (n = 49). When bilayer-integrated GluN1/GluN3A receptors were incubated with 10 μM glycine, the frequency distribution of heights of the particles above the bilayer again showed two peaks, at 3.9 ± 0.2 (n = 44) and 6.0 ± 0.1 nm (n = 56; Fig. 4B). Importantly, the higher peak was significantly lower than that in the control sample (P = 0.004), whereas the lower peak did not change, indicating that the extracellular region had undergone a conformational change upon addition of glycine. A similar reduction in the height of the extracellular domain was seen after addition of 10 μM D-serine (height peaks 3.7 ± 0.2 nm (n = 59) and 5.9 ± 0.1 nm (n = 49; P = 0.006); Fig. 4C). In contrast, glycine did not cause a reduction in height of the extracellular region when added along with DCKA, at either 1 mM (height peaks 3.7 ± 0.2 nm (n = 55) and 6.9 ± 0.2 nm (n = 47; P = 0.639); Fig. 4D) or 10 μM (height peaks 4.0 ± 0.3 nm (n = 63) and 7.1 ± 0.2 nm (n = 55; P = 0.363); Fig. 4E). Further, the height of the extracellular domain was unchanged after addition of 10 μM glutamate (height peaks 4.2 ± 0.2 nm (n = 51) and 6.8 ± 0.1 nm (n = 50; P = 0.120); Fig. 4F).

4. Discussion

Agonist and antagonist action at the GluN1/GluN3 receptor is known to be complex [4,10]. Recombinant GluN1/GluN3 receptors produce only small excitatory currents in response to glycine, likely because of a combination of activation via GluN3 and desensitization via GluN1 [2,3,11]. Indeed, glycine binding to GluN3 alone seems to be sufficient to activate the receptor [3], suggesting that the GluN1 and GluN3 subunits can undergo independent conformational changes. The antagonist DCKA, which binds preferentially to GluN1 [12], likely potentiates receptor function through an inhibition of desensitization. D-serine typically shows little if any measurable agonist activity [2,3], probably because the desensitization it produces overwhelms its agonist effect. When incubated with isolated ABDs, glycine and D-serine have significantly higher affinities for GluN3A than for GluN1 (650-fold and 10-fold, respectively; [12]). The reported EC_{50} for glycine acting on the GluN1/GluN3A receptor expressed in *Xenopus* oocytes was

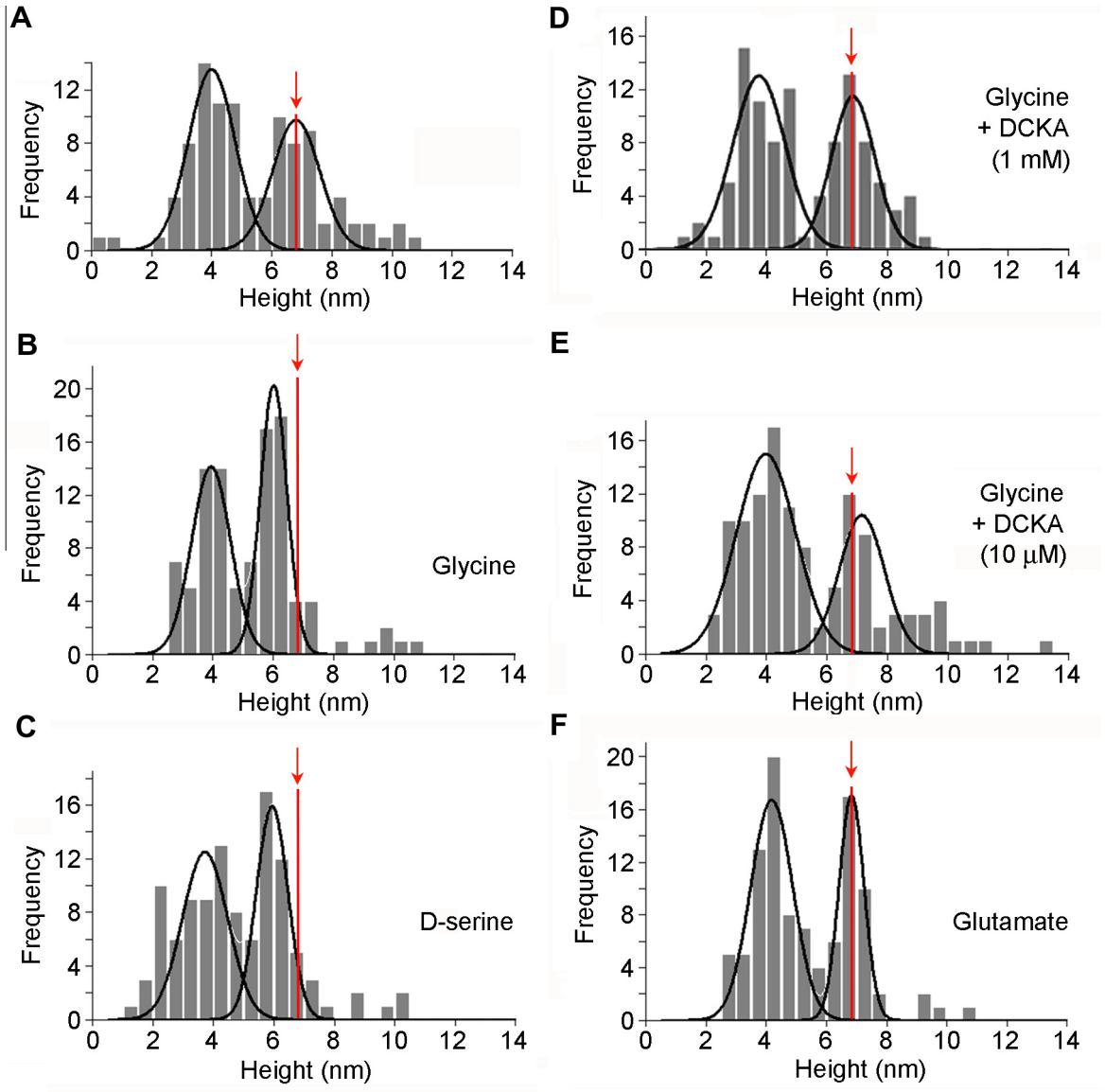

Fig. 4. Activation-induced reduction in height of bilayer-integrated GluN1/GluN3A receptors. (A) Frequency distribution of heights of untreated receptors. Fitted Gaussian curves are overlaid on the histogram. (B–F) Frequency distributions of heights of receptors after treatment with 10 μM glycine (B), 10 μM D-serine (C), 10 μM glycine plus 1 mM DCKA (D), 10 μM glycine plus 10 μM DCKA (E), and 10 μM glutamate (F). The arrows indicate the position of the peak height of the extracellular domain of untreated receptors.

~1 μM, with rapid desensitization occurring at 3 μM and above. At the 10 μM concentrations of glycine and D-serine used in the present study, therefore, we would expect the receptor to exist predominantly in the desensitized state, in which the extracellular domain of the receptor is apparently ~1 nm shorter than in the unstimulated state. Given the measured dissociation constants for DCKA binding to GluN1 and GluN3A (0.54 μM and 647 μM, respectively), we would expect that DCKA would occupy both GluN1 and GluN3A at 1 mM but only GluN1 at 10 μM. In both cases, the desensitization caused by glycine and D-serine should be prevented, but at the lower concentration activation of GluN3A should still occur. The ability of DCKA to block the effect of glycine on the height of the extracellular domain of the receptor at both concentrations is consistent with this scenario, since in both cases GluN1 should remain 'tall'.

The height of the extracellular domain of the GluN1/GluN3A receptor (~7 nm) is about 1 nm shorter than that reported recently for the GluN1/GluN2A receptor [5], perhaps because of differences in the 'flattening' effect of the AFM probe in the two studies, which were carried out using different microscopes. Further, both heights are considerably shorter than the value recently reported for the GluN1/GluN2A NMDA receptor (~11 nm above the membrane; [13,14]). We suggest that the receptor might be more flexible under physiological conditions than in the crystalline state, leading to an increase in its malleability by the scanning probe. Nevertheless, the ~1-nm reduction in height in response to agonist activation was seen with both the GluN1/GluN2A NMDA receptor [5] and the GluN1/GluN3A receptor studied here.

The tendency of GluN1/GluN3A receptor to desensitize rapidly in response to glycine has made it difficult to identify *in vivo*, and there is still some skepticism about whether or not it has a physiological role. Nevertheless, responses to D-serine have been reported in CNS myelin, and these responses were inhibited by the glycine site antagonist 6-cyano-7-nitroquinoxaline-2,3-dione, but not the glutamate antagonist D-2-amino-5-phosphonovalerate

[9]. Further, the responses to D-serine were not seen in NR3A-deficient mice. Although its expression may be restricted, therefore, the GluN1/GluN3A receptor does seem to be functionally active in the CNS. Our results represent the first demonstration of the response of this receptor to activation at the single-molecule level.

Conflict of interest

The authors have no conflicts of interests to disclose.

Acknowledgments

D.B. is a recipient of a David James Bursary from the Department of Pharmacology, University of Cambridge. H.T. holds a Newton International Fellowship. S.S. is supported by the Cambridge International and European Trust. We thank Drs. Pierre Paoletti and David Stroebel (Institut de Biologie de l'École Normale Supérieure (IBENS), Paris, France) for providing the NMDA receptor constructs.

References

[1] S.F. Traynelis, L.P. Wollmuth, C.J. McBain, F.S. Menniti, K.M. Vance, K.K. Ogden, K.B. Hansen, H. Yuan, S.J. Myers, R. Dingledine, Glutamate receptor ion channels: structure, regulation, and function, Pharmacol. Rev. 62 (2010) 405–496.

[2] J.E. Chatterton, M. Awobuluyi, L.S. Premkumar, H. Takahashi, M. Talantova, Y. Shin, J. Cui, S. Tu, K.A. Sevarino, N. Nakahishi, G. Tong, S.A. Lipton, D. Zhang, Excitatory glycine receptors containing the NR3 family of NMDA receptor subunits, Nature 415 (2002) 793–798.

[3] M. Awobuluyi, J. Yang, Y. Ye, J.E. Chatterton, A. Godzik, S.A. Lipton, D. Zhang, Subunit-specific roles of glycine-binding domains in activation of NR1/NR3 *N*-methyl-D-aspartate receptors, Mol. Pharmacol. 71 (2007) 112–122.

[4] S. Pachernegg, N. Strutz-Seebohm, M. Hollmann, GluN3 subunit-containing NMDA receptors: not just one-trick ponies, Trends Neurosci. 35 (2012) 240–249.

[5] Y. Suzuki, T.A. Goetze, D. Stroebel, D. Balasuriya, S.H. Yoshimura, R.M. Henderson, P. Paoletti, K. Takeyasu, J.M. Edwardson, Visualization of structural changes accompanying activation of NMDA receptors using fast-scan AFM imaging, J. Biol. Chem. 288 (2013) 778–784.

[6] D.W. Scott, On optimal and data-based histograms, Biometrika 66 (1979) 605–610.

[7] B.L. Welch, The generalisation of student's problems when several different population variances are involved, Biometrika 34 (1947) 28–35.

[8] O. Söderberg, M. Gullberg, M. Jarvius, K. Ridderstrale, K.J. Leuchowius, J. Jarvius, K. Wester, P. Hydbring, F. Bahram, L.G. Larsson, U. Landegren, Direct observation of individual endogenous protein complexes in situ by proximity ligation, Nat. Methods 3 (2006) 995–1000.

[9] J.C. Piña-Crespo, M. Talantova, I. Micu, B. States, H.-S.V. Chen, S. Tu, N. Nakanishi, G. Tong, D. Zhang, S.F. Heinemann, G.W. Zamponi, P.K. Stys, S.A. Lipton, Excitatory glycine responses of CNS myelin mediated by NR1/NR3 "NMDA" receptor subunits, J. Neurosci. 30 (2010) 11501–11505.

[10] C.-M. Low, S.-L. Wee, New insights into the not-so-new NR3 subunits of *N*-methyl-D-asparate receptor: localization, structure and function, Mol. Pharmacol. 78 (2010) 1–11.

[11] C. Madry, I. Mesic, I. Bartholomäus, A. Nicke, H. Betz, B. Laube, Principal role of NR3 subunits in NR1/NR3 excitatory glycine receptor function, Biochem. Biophys. Res. Commun. 354 (2007) 102–108.

[12] Y. Yao, M.L. Mayer, Characterization of a soluble ligand binding domain of the NMDA receptor regulatory subunit NR3A, J. Neurosci. 26 (2006) 4559–4566.

[13] E. Karakas, H. Furukawa, Crystal structure of a heterotetrameric NMDA receptor ion channel, Science 344 (2014) 992–997.

[14] C.-H. Lee, W. Lü, J.C. Michel, A. Goehring, J. Du, X. Song, E. Gouaux, NMDA receptor structures reveal subunit arrangement and pore architecture, Nature 511 (2014) 191–197.